

# Near-IR imaging of the molecular outflows in HH 24-26, L 1634 (HH 240-241), L 1660 (HH 72) and RNO 15 FIR

C.J. Davis<sup>1</sup>, T.P. Ray<sup>1</sup>, J. Eisloffel<sup>2</sup>, and D. Corcoran<sup>1</sup>

<sup>1</sup> School of Cosmic Physics, Dublin Institute for Advanced Studies, 5 Merrion Square, Dublin 2, Ireland (cdavis@cp.dias.ie, tr@cp.dias.ie)

<sup>2</sup> Thüringer Landessternwarte, Karl-Schwarzschild-Observatorium, D-07778 Tautenburg, Germany (eisloffel@tls-tautenburg.de)

Received 17 July 1996 / Accepted 13 January 1997

**Abstract.** Narrow-band images in H<sub>2</sub> v=1-0 S(1) (2.122 μm) and adjacent continuum (2.104 μm) are presented of a number of outflows that are driven by young, deeply embedded sources. We report the detection of a H<sub>2</sub> outflow associated with the Class 0 source in the HH 24-26 region, HH 24-MMS, as well as extensive H<sub>2</sub> line emission in the HH 25 and HH 26 CO outflows. In L 1634 a sequence of well-defined molecular bow shocks in the blue-shifted outflow lobe points to variability in the flow velocity, while in L 1660, the poorly aligned H<sub>2</sub> knots suggest a wide outflow opening angle and perhaps also a variable flow direction. We also report the discovery of a highly collimated molecular jet associated with the embedded source RNO 15 FIR.

These observations provide evidence that molecular outflows from young stars are driven by collimated jets. Indeed, in H<sub>2</sub>, we likely observe the molecular shocks which sweep up ambient gas to form the associated CO outflows. We find, however, no obvious correlation between the presumed age of the source of each outflow (based on its IR excess), and the length or luminosity of the flow in H<sub>2</sub>.

**Key words:** ISM: jets and outflows – infrared: ISM: lines and bands – ISM: HH 24-26; L 1634 (HH 240-241); L 1660 (HH 72); RNO 15 FIR

## 1. Introduction

There is a growing body of observations that indicate that the massive (CO) outflows associated with young stellar objects are driven by highly collimated jets (e.g. Davis & Eisloffel 1995; McCaughrean, Rayner & Zinnecker 1994; Zinnecker, McCaughrean & Rayner 1996; see also the review of Bachiller 1996). This interaction probably takes place via molecular shocks which develop along the length of each jet, perhaps in a turbulent boundary (or mixing) layer, or in bow shocks at the head of each jet. These non-dissociating, low-velocity shocks ( $V_{\text{shock}} < 30\text{--}50 \text{ km s}^{-1}$ ) are best observed in the ro-vibrational lines of H<sub>2</sub>. Because of their efficient radiative cooling, they are very much transient features which illustrate only the current

shock-activity in any one source. Essentially we are seeing the “sparks that fly” as the jet interacts with its surroundings. Nevertheless, near-IR images of star-forming regions do provide constraints on outflow structure and morphology, such as flow collimation and variability. They may also lead to the discovery of new outflows, identify the probable location of outflow sources, and help clarify the complex flow morphology seen in low resolution CO observations. Observing molecular (H<sub>2</sub>) shocks in outflows may also allow us to distinguish between entrainment models.

Motivated by these ideas, we have imaged a number of potentially very young outflow systems, in H<sub>2</sub> v=1-0 S(1) line emission (hereafter referred to as H<sub>2</sub> S(1)) and adjacent continuum. These flows are driven by deeply embedded sources that are not observed directly at near-IR wavelengths. Indeed, the HH 24-MMS outflow source is identified as a bona fide Class 0 source, i.e. a source with a bolometric-to-submillimeter luminosity ratio of  $\leq 400$  (André, Ward-Thompson & Barsony 1993). Specifically, images of HH 24-26, L 1634 (HH 240-241), L 1660 (HH 72) and RNO 15 FIR are presented. Our images of HH 24-26 are also compared to published CO outflow maps, and new CO J=3-2 data of the L 1634 outflow are discussed.

## 2. Observations

Near-infrared images were obtained with the 1–5 μm imaging camera IRCAM 3 on the 3.8 m U.K. Infrared Telescope (UKIRT) on December 17–19 1994. IRCAM 3 is fitted with a 256×256 pixel NICMOS 3 InSb array. The default pixel scale of 0.286"/pixel was used, which yields a field-of-view of 73"×73". Mosaics covering the outflow regions (in each case with the frames overlapping by ~13") were obtained through a narrow-band H<sub>2</sub> v=1-0 S(1) filter ( $\lambda = 2.122 \mu\text{m}$ ,  $\Delta\lambda(\text{FWHM}) = 0.020 \mu\text{m}$ ); similar mosaics were obtained with an adjacent continuum filter ( $\lambda = 2.104 \mu\text{m}$ ,  $\Delta\lambda(\text{FWHM}) = 0.020 \mu\text{m}$ ). Both filters are free of strong atmospheric OH lines and are situated in a part of the K-band where the atmospheric transmission is high. The integration time per individual frame was 60 sec (sufficient for background-limited operation); the total on-source integration time towards the HH 24

Send offprint requests to: C.J. Davis

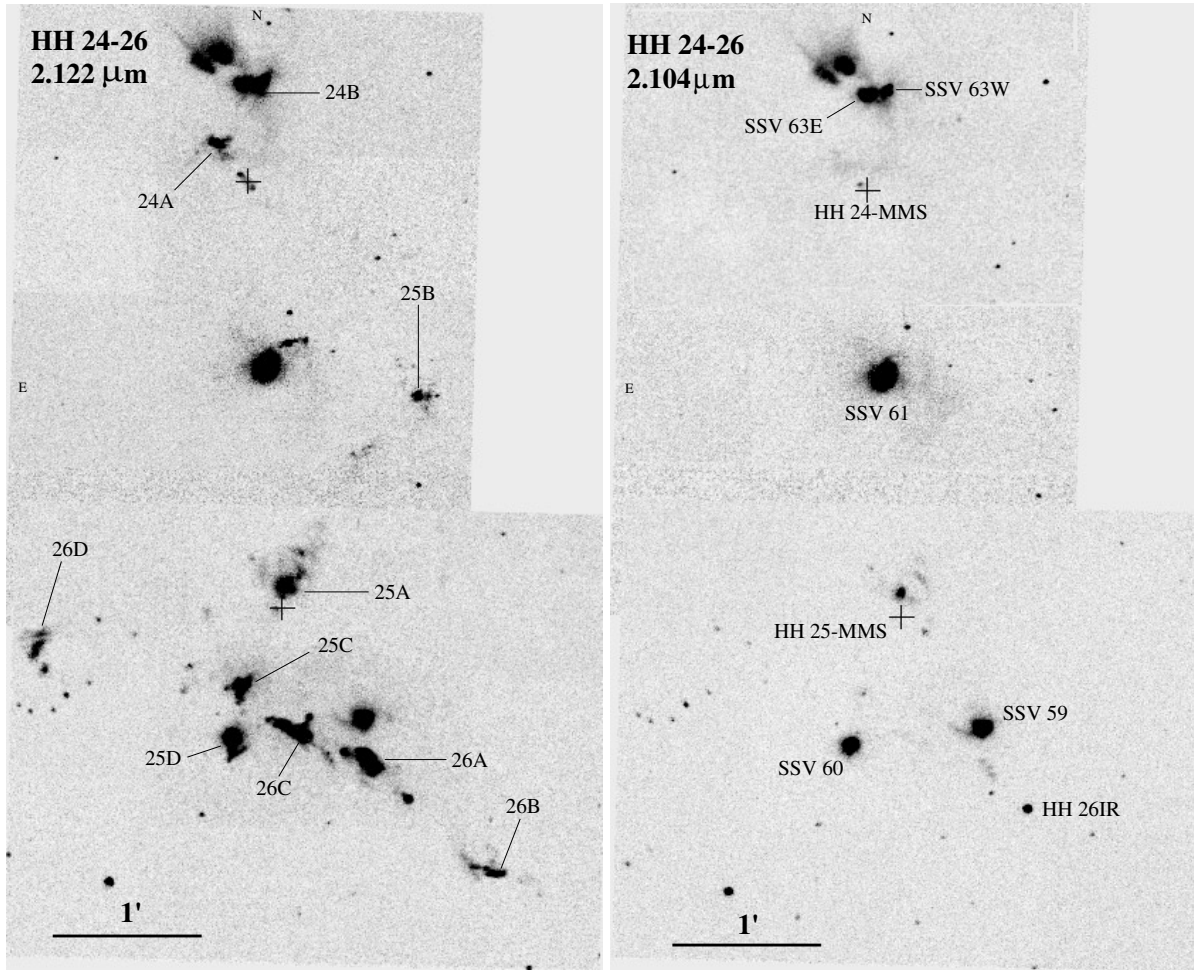


**Fig. 1.** Narrow-band images, at  $2.122\mu\text{m}$  ( $\text{H}_2$  + continuum) and  $2.104\mu\text{m}$  (continuum), of the HH 24-26 region. The two crosses mark the positions of the Class 0 source HH 24-MMS and the Class 0/Class I source HH 25-MMS.

and HH 26 regions were 3 mins and 5 mins respectively per filter. The on-source integration times towards L 1660, L 1634 and RNO 15 FIR were similarly 4–5 mins.

To reduce the data, a sky frame was computed for each object frame from between 4 and 7 adjacent (in time) spatially shifted object frames: the median average of these frames was used so that the emission from any stars or extended objects was completely removed. By subtracting this sky from the object frame the dark current is also removed. We used the same (normalised) sky for flat-fielding, though it was then necessary to subtract a dark frame (of equal integration time) from the sky. Observations of the UKIRT faint standard stars FS 2 ( $K = 10.50^{\text{m}}$ ) and FS 9 ( $K = 8.27^{\text{m}}$ ) were also made, at the beginning of each night, to flux calibrate the images.

CO J=3-2 spectra towards L 1634 were obtained through the Service Observing Program of the James Clerk Maxwell Telescope on February 12 1996. The common user receiver RxB3i and the DAS spectrometer were used. 41 spectra were observed in total, along a strip orientated at a position angle of  $110^\circ$ . The grid spacing along the strip was  $10''$ ; the JCMT beam

(FWHM) at the CO 3-2 frequency (345.813 GHz) is  $14''$ . Frequency switching was employed; a switch of 24.34 MHz (every 2 sec) produced spectra free of interference. The system temperature was measured to be 1800 K. The data were reduced using the SPECX package.

### 3. Results

#### 3.1. The HH 24-26 region

The Herbig-Haro (HH) objects 24, 25 and 26 are situated a few arcminutes south of NGC 2068 within the L 1630 dark cloud (distance  $\sim 400$  pc; Anthony-Twarog 1982). HH 24 represents a complex of at least 3 collimated optical outflows (Mundt, Ray & Raga 1991), while HH 25 and HH 26 appear as more nebulous HH objects a few arcminutes to the south (Jones et al. 1987). Submillimetre and radio maps of the region extend north-south over roughly  $6'$  (Gibb & Heaton 1993; Verdes-Montenegro & Ho 1996). Four of these cores harbour VLA continuum sources, all of which are believed to be young stellar objects (Bontemps, André &

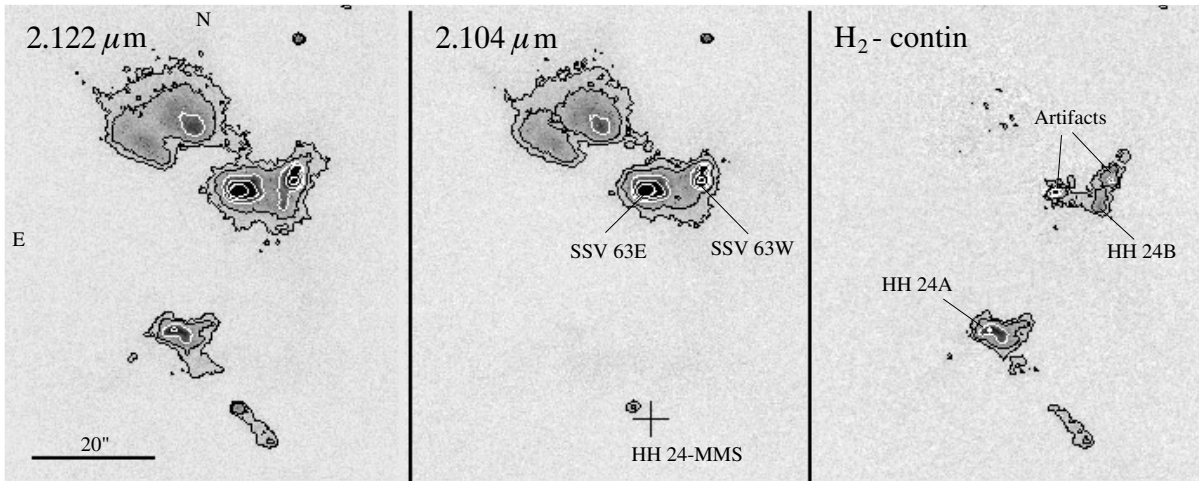


**Fig. 2.** H<sub>2</sub> S(1) + continuum, continuum and pure H<sub>2</sub> S(1) images of HH 24. The black contours measure 1 and  $2 \times 10^{-18} \text{ W m}^{-2} \text{ arcsec}^{-2}$ ; the white contours measure 5, 10, 25 and  $200 \times 10^{-18} \text{ W m}^{-2} \text{ arcsec}^{-2}$ .

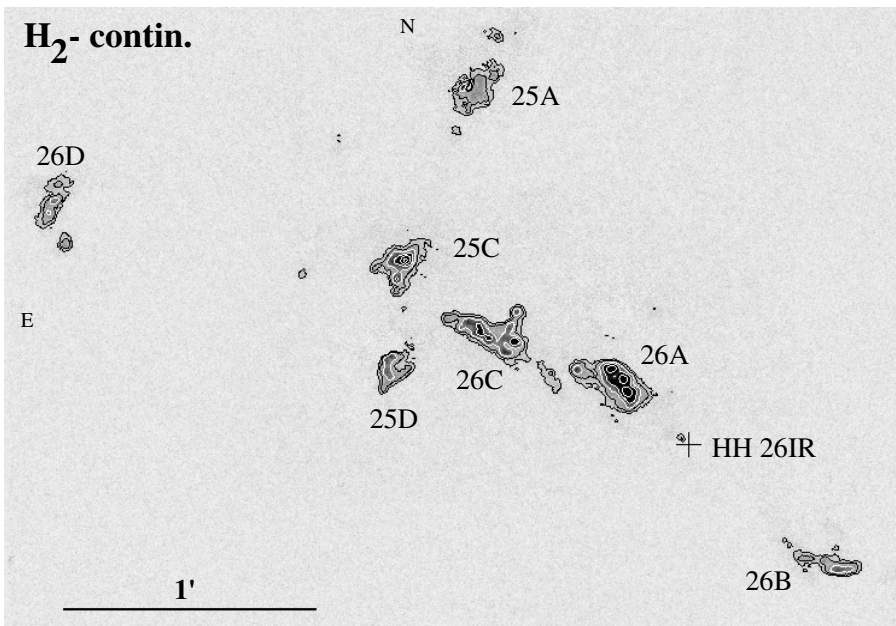


**Fig. 3.** Continuum-subtracted H<sub>2</sub> S(1) image of the HH 26 outflow region. The bright IR sources SSV 59 and SSV 60 were fit (with 2-D gaussians) and removed from the  $2.122 \mu\text{m}$  and  $2.104 \mu\text{m}$  images before the latter was subtracted from the former. Residual artifacts in the resulting image were masked and replaced with gaussian noise. Thus, any H<sub>2</sub> emission that was superimposed onto either source is lost. The black contours measure 1 and  $2 \times 10^{-18} \text{ W m}^{-2} \text{ arcsec}^{-2}$ ; the white contours start at  $4 \times 10^{-18} \text{ W m}^{-2} \text{ arcsec}^{-2}$  and increase in multiples of 2.

Ward-Thompson 1995). Two of these (SSV 61 and SSV 63) appear in the  $2.2 \mu\text{m}$  survey of Strom, Strom & Vrba (1976), and are clearly evident in the near-infrared images presented in Fig. 1. SSV 61 is recognised as a classical T Tauri star; the two SSV 63 sources, SSV 63E and SSV 63W, are Class I embedded IR sources, although here SSV 63W is resolved into two components (see Fig. 2). Conversely, the two remaining VLA sources, which are identified with HH 24-MMS and HH 25-MMS, are not detected in the near-IR. These are more heavily embedded and presumably less evolved than their near-infrared neighbours; HH 24-MMS and HH 25-MMS are believed to be Class 0 and Class 0/extreme-Class I sources respectively (Bontemps et al. 1995; Ward-Thompson et al. 1995; Chandler et al. 1995).

The narrow-band images presented in Fig. 1 reveal at least five distinct outflows, all of which appear to be randomly orien-

tated. Four of these are identified with HH 24A, HH 24B, HH 25 and HH 26, though we also observe a cusp of H<sub>2</sub> emission extending northwestward from SSV 61. The images reveal a number of shock regions which are not evident in optical images of the outflows, particularly towards HH 25 and HH 26. The integrated fluxes and positions (measured as offsets relative to the VLA position of SSV 61) of the main H<sub>2</sub> features in Fig. 1 are listed in Table 1. The coordinates are subject to inaccuracies in the mosaicing, and are thought to be accurate to within  $1''$ – $2''$ .

### 3.1.1. HH 24

In Fig. 2 we show narrow-band images of just the HH 24 region, together with a continuum-subtracted H<sub>2</sub> S(1) image. Although HH 24 is well known as a site of very active outflow activity

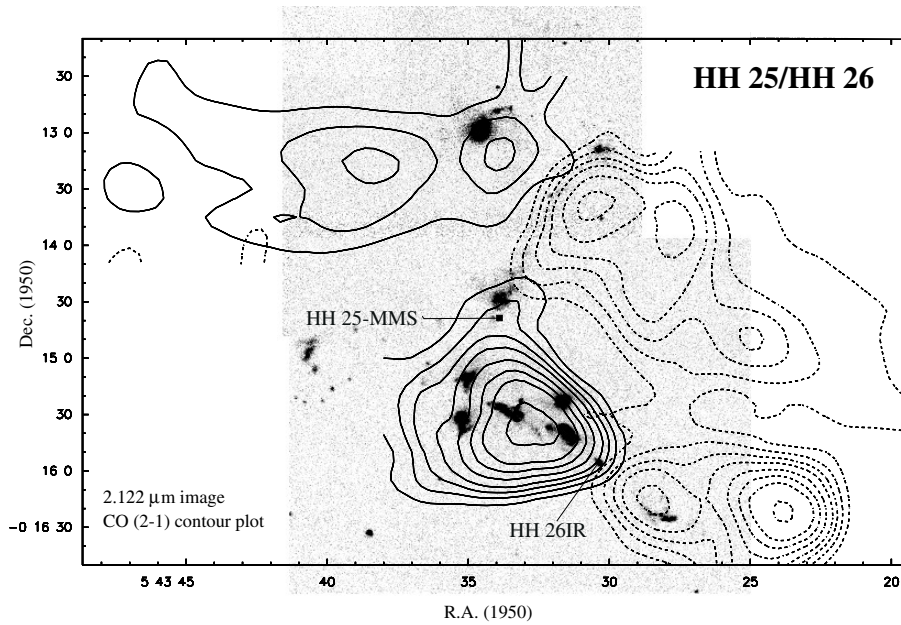


**Fig. 4.** H<sub>2</sub> (+ continuum) image of the HH 25 and HH 26 outflows with, superimposed, a contour plot showing the CO J=2-1 outflows mapped by Gibb & Heaton (1993). The full contours show the blue-shifted CO gas, the dashed contours the red-shifted gas.

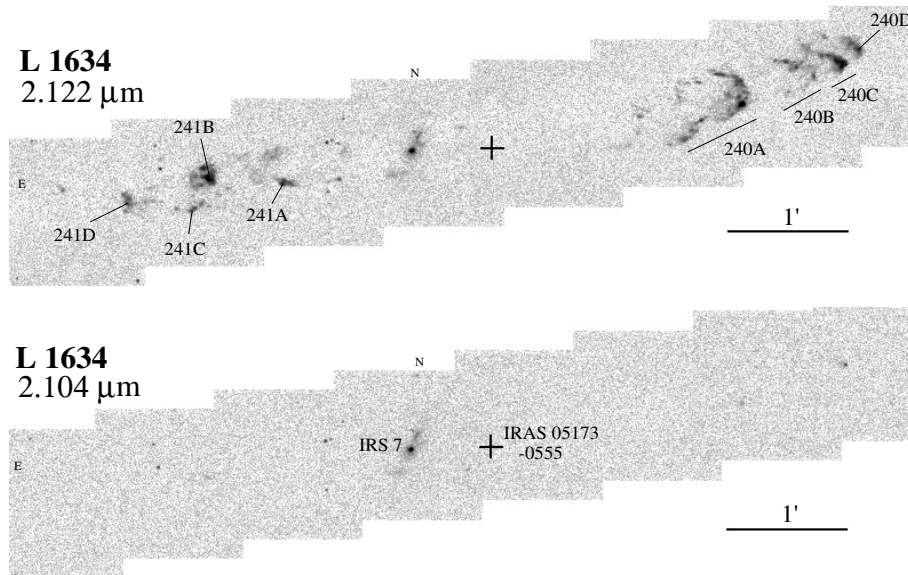


**Fig. 5.** Narrow-band images, at 2.122  $\mu\text{m}$  (H<sub>2</sub> + continuum) and 2.104  $\mu\text{m}$  (continuum), of the L 1634 outflow. The previously known optical HH objects RNO 40 and RNO 40E are here labelled HH 240A and HH 241A respectively. IRAS 05173-0555, the driving source of the outflow, is marked with a cross.

(Mundt et al. 1991; Solf 1987), we observe just a few H<sub>2</sub> emission features here (see also Zealey et al. [1992]). The bright, optically-visible HH object HH 24A appears arc-shaped in H<sub>2</sub> and notably extends towards a “jet-like” H<sub>2</sub> feature some 20'' to the southwest (for a comparison of optical and near-IR images of this region see Zealey et al. [1992]). This “H<sub>2</sub> jet” is probably part of an outflow from the Class 0 source HH 24-MMS, which lies on the jet axis. Bontemps, Ward-Thompson & André (1996) have also recently observed this “mini-jet” in H<sub>2</sub> S(1) and at 3.6 cm with the VLA.

HH 24A marks the point where the HH 24-MMS jet and the more extended, HH 24C-E optical jet appear to cross (the axis of the HH 24C-E jet, which is orientated at a P.A.  $\sim 155^\circ$  E of N, passes through a point  $\sim 2''$  to the west of the IR peak associated

with SSV 63E). The proper motion studies of Jones et al. (1987) suggest that HH 24A is moving towards the southwest: it is unlikely, therefore, that HH 24A is powered by HH 24-MMS. Indeed, Jones et al. (1987) and Solf (1987) argue that HH 24A is part of the HH 24C-E jet, and that it traces the shocked edge of the high density clump observed by Chini et al. (1993) which harbours HH 24-MMS.

### 3.1.2. HH 25/HH 26

The HH 25 and HH 26 outflows are particularly striking in Fig. 1, being almost orthogonal to one another. It is tempting to suggest that knot HH 25C represents a zone of interaction where the outflows cross one another, given its position and the fact that it is extended along both HH 25 and HH 26 out-

**Table 1.** Coordinates and photometry for the H<sub>2</sub> S(1) line-emission features in the HH 24, HH 25 and HH 26 outflows. Positions are measured relative to the VLA coordinates of SSV 61; R.A.(1950)= 05<sup>h</sup> 43<sup>m</sup> 34<sup>s</sup>.4, Dec(1950)= -00° 13′ 03″ (Bontemps et al. 1995).

	RA (1950)	DEC (1950)	$I_{\text{integ}}$ ( $\times 10^{-16} \text{W m}^{-2}$ )
HH 24A	05 43 35.8	-00 11 31	1.9
HH 24B	05 43 34.5	-00 11 10	~0.5
HH 25A	05 43 33.9	-00 14 32	2.7
HH 25B	05 43 30.3	-00 13 15	1.2
HH 25C	05 43 35.0	-00 15 13	4.7
HH 25D	05 43 35.3	-00 15 39	1.8
HH 26A	05 43 31.6	-00 15 44	9.1
HH 26B	05 43 28.2	-00 16 30	1.8
HH 26C	05 43 35.5	-00 15 33	5.9
HH 26D	05 43 40.6	-00 14 57	1.8

flow axes (see also the continuum-subtracted image in Fig. 3). However, clearly neither flow is diverted nor *decollimated* beyond this point, so the two flows probably do not interact here. The sequence of emission features in both HH 25 and HH 26 describe smooth arcs. A similar curving flow geometry is evident in L 1448 (Davis et al. 1994a). Like L 1448, the curves in HH 25 and HH 26 may be due to ambient density gradients or large scale magnetic fields. Alternatively, they may reflect the proper motions of their sources.

Recent 3.6 cm continuum observations have failed to detect a source associated with the HH 26 outflow, above a  $5\sigma$  noise level of  $\sim 100 \mu\text{Jy beam}^{-1}$  (A.G. Gibb, 1996, private communication). However, the likely outflow source is evident in our images. About 20″ southwest of HH 26A there is a near-IR source which 1) lies on the outflow axis, 2) is at the geometric centre of the HH 26 CO outflow (Gibb & Heaton 1993), and 3) is, in the H<sub>2</sub> image, slightly extended along the outflow direction. The coordinates of this star, which we shall refer to as HH 26IR, are R.A.(1950)= 05<sup>h</sup> 43<sup>m</sup> 30<sup>s</sup>.5, Dec.(1950)= -00° 15′ 59″ (measured relative to the position of SSV 61 in our mosaic). The nearest IRAS source, IRAS 05435-0015 is offset by (9″, 31″) from this position; IRAS 05435-0015 is very likely associated with SSV 59. The magnitude at K of HH 26IR, estimated from its flux density measured at 2.104  $\mu\text{m}$ , is 11.7( $\pm 0.7$ ). By comparison, the magnitudes of SSV 59, SSV 60 and SSV 61, estimated in the same way, agree to within 0.3<sup>m</sup> with those given by Strom et al. (1976).

The obvious association between the near-infrared HH knots in HH 25 and HH 26 and the outflows mapped in CO J=2-1 emission by Gibb & Heaton (1993) is quite striking. Indeed, the slightly confusing picture presented by the CO maps alone is clarified when a comparison is made with the near-infrared data (Fig. 4). In both HH 25 and HH 26 we see a perfect alignment between the HH knots and the associated CO outflows. The northerly extension of the blue-shifted lobe of the almost east-

west HH 26 CO outflow (near HH 25A) is almost certainly due to the overlapping HH 25A outflow here, as is the bump on the southern side of the blue-shifted HH 26 lobe. These overlapping outflows are somewhat more apparent in the more recent, higher-resolution, CO J=3-2 maps of Gibb & Davis (1997). Note also that, as one would expect, the brightest H<sub>2</sub> knots from both the HH 25 and HH 26 outflows are coincident with the *blueshifted* molecular (CO) lobes, implying that extinction effects may be important even in the K band.

### 3.2. L 1634 (HH 240-241)

Although L 1634 appears in Fukui’s (1989) list of outflow sources, to date no CO maps have appeared in the literature. L 1634 itself is a dark cloud in Orion with an assumed distance of 500 pc (Hilton & Lahulla 1995). The core is perhaps better known as the site of the HH object RNO 40 (Jones et al. 1984; Bohigas, Persi & Tapia 1993; recently designated HH 240 in the catalogue of Reipurth 1994).

Our near-infrared images of the region reveal many bright H<sub>2</sub> line emission knots along the outflow. In Fig. 5 we show both H<sub>2</sub> S(1) line and nearby continuum images of this area. From these we see that all of the extended, filamentary knots and clumps along the flow axis are indeed H<sub>2</sub> line emission features, the exception being the S-shaped wisp around the infrared source, here labelled IRS 7 (labelled as such to avoid confusion with the IRS sources in Bohigas et al. [1993], and in keeping with the nomenclature of Hodapp & Ladd [1995]). Indeed, this star was thought to be a possible candidate exciting source for the outflow. However, we have recently obtained a strip of CO J=3-2 spectra in service time on the James Clerk Maxwell Telescope. We present these data in the form of a position-velocity diagram in Fig. 6. Unfortunately, the axis of the strip map was not well aligned with the outflow axis. However, the data clearly point to the origin of the outflow being about 50″ to the west of IRS 7. At this position there is an IRAS source (IRAS 05173-0555) which had previously been detected by Cohen, Harvey & Schwartz (1985) at far-infrared wavelengths. The source has a steeply rising spectral energy distribution through the IRAS bands. Reipurth et al. (1993) have also measured the source flux at 1300  $\mu\text{m}$ ; they confirm that it is deeply embedded ( $L_{\text{bol}} \sim 17 L_{\odot}$ ). There is thus little doubt that IRAS 05173-0555 drives this spectacular outflow.

IRS 7 may also power a molecular outflow; Hodapp and Ladd (1995) found two faint, H<sub>2</sub> line-emission features about 90″ to the southeast and northwest of this source. These features are outside the area covered by our images, so we cannot confirm their presence. However, we do detect blue-shifted CO emission towards IRS 7 which may well be part of such an outflow (IRS 7 coincides with the red-shifted lobe of the east-west L 1634 CO outflow; see Fig. 6).

The H<sub>2</sub> features to the east of the exciting source (HH 241A-D) reside in the red-shifted lobe of the CO outflow; those to the west of the source (HH 240A-D) are in the blue-shifted lobe (A. Mizuno, 1996, private communication; see also Fig. 6). The western lobe of the outflow has previously been imaged at op-

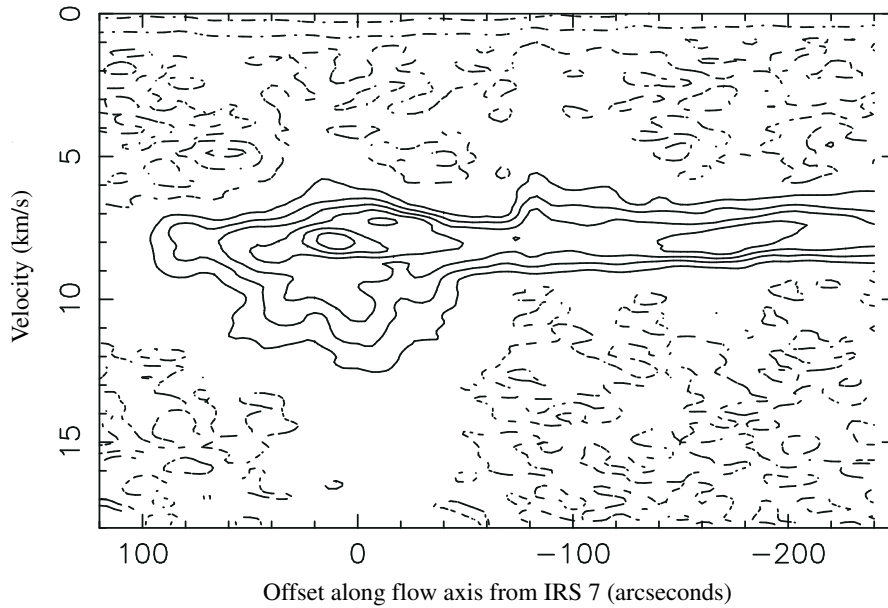


**Fig. 6.** A CO J=3-2 position-velocity map of L1634. The zero offset position is that of the previously suspected source IRS 7 (R.A.(1950)= 05<sup>h</sup> 17<sup>m</sup> 24<sup>s</sup>.7, Dec(1950)= -5° 55' 08''). However, these data suggest that the driving source is in fact situated some 50'' west of this position. The map was orientated at a p.a. = 110° (note that the flow axis has a p.a. ~ 100°).

**Table 2.** Coordinates and photometry for the H<sub>2</sub> S(1) line-emission features in the L 1634 (HH 240-241) outflow. The coordinates are of the brightest H<sub>2</sub> peak in each feature, and are measured relative to IRS7 (Hodapp & Ladd 1995).

	RA (1950)	DEC (1950)	$I_{\text{peak}}$ ( $\times 10^{-18} \text{W m}^{-2} \text{arcsec}^{-2}$ )	$I_{\text{integ}}$ ( $\times 10^{-16} \text{W m}^{-2}$ )
HH 240A	05 17 13.5	-5 54 43	13.8	4.1
HH 240B	05 17 11.7	-5 54 24	2.6	1.1
HH 240C	05 17 10.1	-5 54 22	6.8	2.1
HH 240D	05 17 9.6	-5 54 15	3.8	1.0
HH 241A	05 17 30.1	-5 55 24	4.0	1.0
HH 241B	05 17 31.3	-5 55 20	9.0	2.5
HH 241C	05 17 31.9	-5 55 35	1.8	0.4
HH 241D	05 17 34.2	-5 55 33	2.0	0.7

tical (Jones et al. 1984; Bohigas et al. 1993) and near-IR (J,H and K) wavelengths (Bohigas et al. 1993), although Schwartz, Cohen & Williams (1987) were the first group to detect H<sub>2</sub> line emission here. The H<sub>2</sub> feature nearest the outflow source coincides with an optically visible HH object, RNO 40 (HH 240A), although its true bow shock nature was not evident in these optical data.

Jones et al. (1984) measured a large proper motion for HH 240A (RNO 40) directed away from the IRAS source. They also identified a faint HH object, RNO 40E to the east of the IRAS source which also coincides with a H<sub>2</sub> knot, HH 241A. Jones et al. measured the proper motion of HH 241A and found that it was also moving away from the IRAS source. These HH knots, together with some of the other bright H<sub>2</sub> features in the L 1634 outflow, are labelled in Fig. 5; their coordinates (accurate to ~ 1''– 2'') and fluxes are listed in Table 2.

It is interesting to note that the eastern and western lobes of the L 1634 outflow, as traced in H<sub>2</sub>, are equal in length. The distance on the sky from IRAS 05173-0555 to HH 240D

and HH 241D is 180'' (0.40 pc) and 173'' (0.39 pc) respectively. Also, for each of the bright H<sub>2</sub> structures in the western lobe (HH 240A-D), there is an “equivalent” structure, at roughly the same distance from the IRAS source, in the eastern lobe (HH 241A-D). HH 240A-D appear as a series of molecular bow shocks, similar to those seen in for example the Cepheus A outflow (Hartigan et al. 1996). However, unlike Cep A, where the bows are clustered in a chaotic group, in L 1634, the bow shocks appear periodically along the outflow axis. Indeed, it is tempting to suggest that the L 1634 outflow may be variable, and particularly that the H<sub>2</sub> bows may be the result of a “pulsed” jet (e.g. Raga et al. 1990; Gouveia dal Pino & Benz 1994). Variable jets will be discussed further in Sect. 4.2, where we show that the variable jet models are, at least to some degree, supported by the H<sub>2</sub> data in L 1634.

### 3.3. L 1660 (HH 72)

At a distance of ~1500 pc (Hilton & Lahulla 1995), L 1660 is one of a number of bright-rimmed, diffuse cores which surround

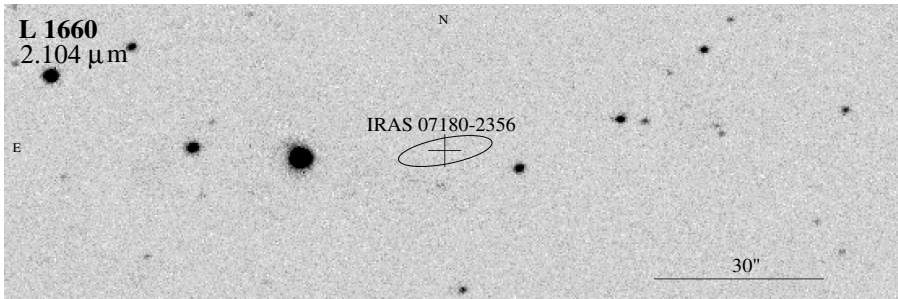
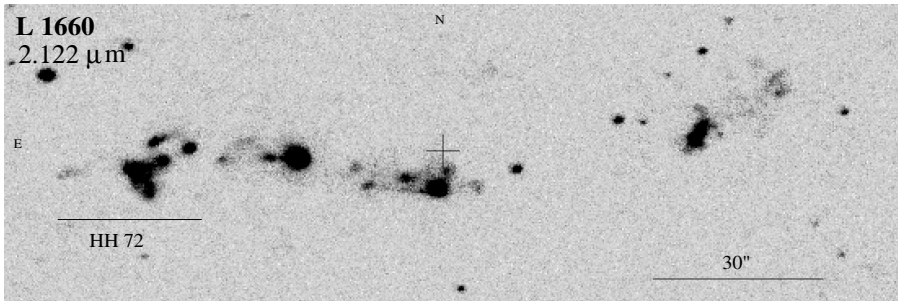


**Fig. 7.** Narrow-band images, at  $2.122\mu\text{m}$  ( $\text{H}_2$  + continuum) and  $2.104\mu\text{m}$  (continuum), of the L 1660 outflow. The optically visible portion of the outflow, HH 72, is indicated. The IRAS source that possibly powers the outflow is marked with a cross in each image. Its coordinates are R.A.(1950)=  $07^{\text{h}} 18^{\text{m}} 00^{\text{s}}.9$ , Dec(1950)=  $-23^{\circ} 56' 42''$ . The  $1\sigma$  IRAS error ellipse is also shown.

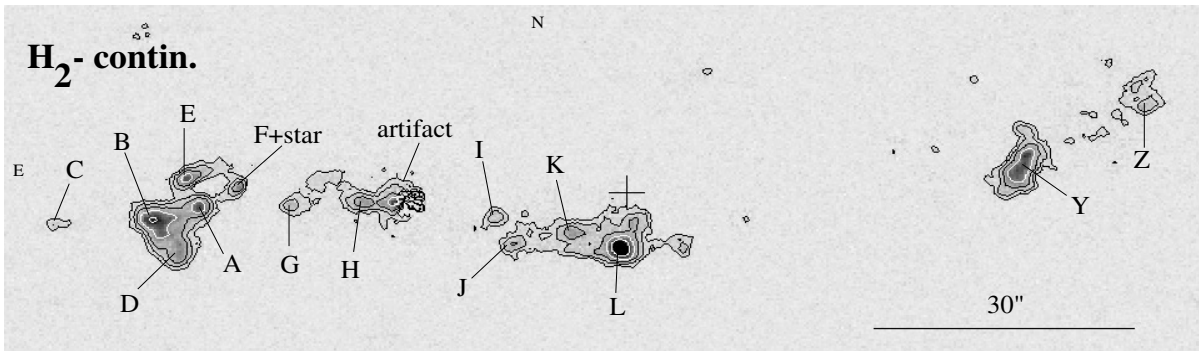


**Fig. 8.** A continuum-subtracted  $\text{H}_2$  S(1) image of the L 1660 (HH 72) outflow. The black contours measure  $0.5, 1$  and  $2 \times 10^{-18} \text{ W m}^{-2} \text{ arcsec}^{-2}$ ; the white contours start at  $4 \times 10^{-18} \text{ W m}^{-2} \text{ arcsec}^{-2}$  and increase in multiples of 2. The artifact results from the poor subtraction of the bright star at this position (see Fig. 7), though the emission to the east of this artifact (knot H) is clearly  $\text{H}_2$  S(1) line emission. The position of IRAS 07180–2356 is again marked with a cross.

the young OB cluster NGC 2362 in Vela (Reipurth & Graham 1988). Schwartz, Gee & Huang (1988) found an east-west bipolar molecular outflow here, driven by the luminous IRAS source 07180–2356 ( $L_{\text{bol}} \sim 170 L_{\odot}$ ; Reipurth et al. 1993). About the same time, Reipurth & Graham (1988) observed a string of optical HH knots (HH 72 A–C) near the eastern edge of the L 1660 core. These HH knots appear near the end of the red lobe of the CO outflow, where they clearly delineate the outflow as it leaves the core.

In Fig. 7 we show narrow-band images of the L 1660 region, at  $2.122\mu\text{m}$  and  $2.104\mu\text{m}$ . The morphology of the individual  $\text{H}_2$  features is evident in the continuum-subtracted  $\text{H}_2$  contour plot in Fig. 8 (here we continue the labelling scheme of Reipurth & Graham 1988).

In addition to the HH knots HH 72A–C, there are a number of other shock features within the L 1660 core which were ob-

served in  $\text{H}_2$ . These may well be obscured from view at optical wavelengths. Many of the background reference stars in our mosaic are evident on the Digitised Sky Survey image of the same region. We were therefore able to measure the positions of the  $\text{H}_2$  knots to an accuracy of better than  $1''$ . The coordinates are listed in Table 3, together with an integrated flux measurement for each knot. We were also able to accurately mark the position of IRAS 07180–2356 on our images.

Surprisingly, the  $\text{H}_2$  features in L 1660 (Figs. 7 & 8) do not lie on a common axis, although like the molecular outflow traced in CO they extend in roughly an east-west direction (Schwartz et al. 1988). The outflow, traced in  $\text{H}_2$ , certainly appears to be poorly collimated. If we assume that the outflow source lies closer to knot L than is suggested by the IRAS source position and  $1\sigma$  error ellipse, and if the  $\text{H}_2$  knots delineate the (northern) edges of the blue and red-shifted molecular outflow lobes,

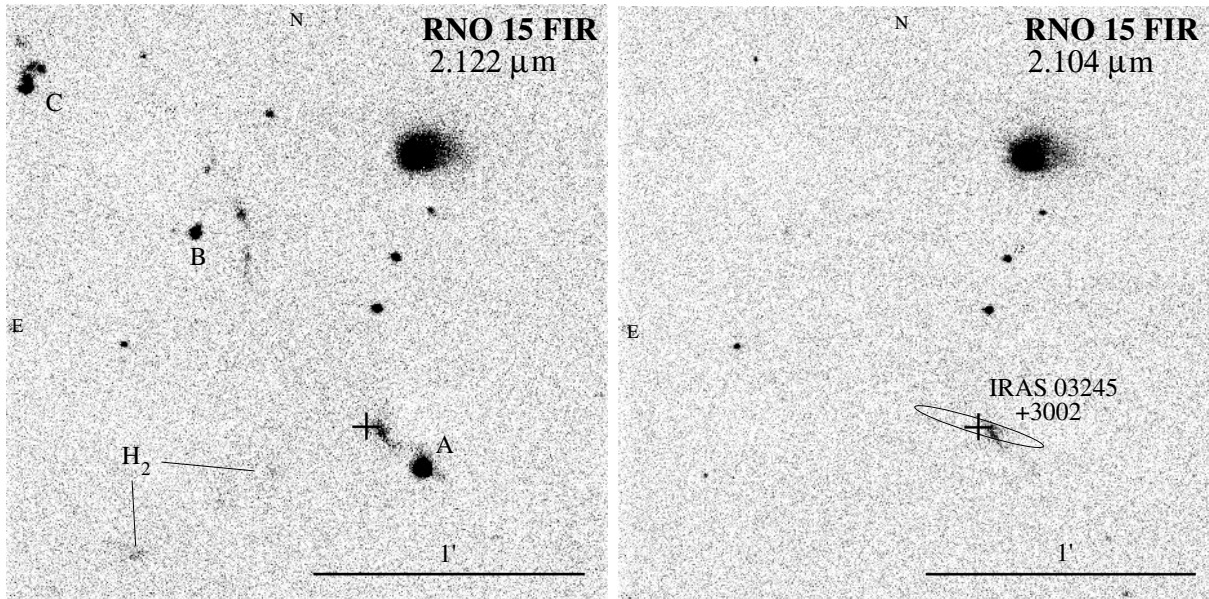


**Fig. 9.** Narrow-band images, at 2.122  $\mu\text{m}$  (left) and 2.104  $\mu\text{m}$  (right), of the RNO 15 FIR outflow (knots A-C). The cross marks the IRAS position of the exciting source. The  $1\sigma$  IRAS error ellipse is also shown.

**Table 3.** Coordinates and photometry for the  $\text{H}_2$  S(1) line-emission features in the L 1660 (HH 72) outflow.

	RA (1950)	DEC (1950)	$I_{\text{integ}}^{\text{a}}$ ( $\times 10^{-16} \text{ W m}^{-2}$ )
HH 72A	07 18 04.47	-23 56 42.5	0.34
HH 72B	07 18 04.79	-23 56 43.9	0.75
HH 72C	07 18 05.66	-23 56 44.2	0.03
HH 72D	07 18 04.65	-23 56 47.2	0.26
HH 72E	07 18 04.54	-23 56 39.0	0.22
HH 72G	07 18 03.67	-23 56 42.6	0.07
HH 72H	07 18 03.08	-23 56 42.4	0.19
HH 72I	07 18 01.99	-23 56 44.9	0.07
HH 72J	07 18 01.83	-23 56 48.0	0.11
HH 72K	07 18 01.33	-23 56 46.9	0.20
HH 72L	07 18 00.95	-23 56 48.8	0.84
HH 72Y	07 17 57.60	-23 56 40.7	0.84
HH 72Z	07 17 56.54	-23 56 33.7	0.22

<sup>a</sup>Measured in a  $5''$  aperture (centred on each peak), except knots Y and Z, where an  $11''$  aperture was used.

then the opening angle of the flow would be about  $25^\circ$ – $30^\circ$ . In addition to being poorly collimated, the outflow may also be variable, particularly in direction (we discuss this possibility further in Sect. 4.2). However, we should not discount the possibility that the  $\text{H}_2$  knots in L 1660 derive from two independent outflows, which appear projected against one another on the sky. In this scenario, knots E–L could be part of a collimated, knotty,  $\text{H}_2$  jet from an undetected source, while the remaining features could be powered by IRAS 07180–2356. A similar situation is observed in L 1448, where the L 1448-mm

**Table 4.** Coordinates and photometry for the  $\text{H}_2$  S(1) line-emission features in the RNO 15-FIR outflow.

	RA (1950)	DEC (1950)	$I_{\text{peak}}$ ( $\times 10^{-18}$ $\text{W m}^{-2} \text{ arcsec}^{-2}$ )	$I_{\text{integ}}$ ( $\times 10^{-16}$ $\text{W m}^{-2}$ )
A	03 24 33.9	30 02 27	7.7	0.67
B	03 24 37.8	30 03 19	4.2	0.15
C	03 24 40.7	30 03 53	5.1	0.39

and L 1448-IRS 3 outflows are virtually parallel and overlapping in projection (Bachiller et al. 1990; Davis & Smith 1995).

### 3.4. RNO 15-FIR

RNO 15 is an emission line star which appears on the Palomar POSS plates as a faint, nebulous object associated with a dark cloud in L 1455 (distance  $\sim 350$  pc; Herbig & Jones 1983). RNO 15 FIR on the other hand, which is situated  $\sim 2'$  northwest of RNO 15, is not visible on the Palomar plates, although both stars were detected by the IRAS satellite (IRAS 03247+3001 and 03245+3002 respectively). Goldsmith et al. (1984) and later Levreault (1988) have mapped this region in CO; both groups find evidence for at least three molecular outflows within a  $12' \times 12'$  area (note that Levreault [1988] refers to RNO 15 FIR as L 1455 FIR). RNO 15 clearly drives a bipolar molecular flow in a northwest-southeasterly direction. RNO 15 FIR also powers a molecular outflow, though only the westerly, blue-shifted lobe was clearly observed. The red-shifted lobe probably overlaps with the red lobe of the RNO 15 outflow, the two being indistinguishable in the relatively low resolution data of Levreault (1988) and Goldsmith et al. (1984).

In Fig. 9 we show narrow band H<sub>2</sub> S(1) (+ continuum) and adjacent continuum images of the RNO 15 FIR region. Using the K' image of Hodapp (1994) we were able to measure the positions of the main H<sub>2</sub> knots seen here, and also accurately position RNO 15 FIR on each image. In these images we see a patch of diffuse, continuum emission close to RNO 15 FIR. We also observe a number of bright, though compact H<sub>2</sub> knots which lie along an axis common to both RNO 15 FIR and the reflection nebula. We label these A-C. These features clearly suggest the presence of a highly collimated outflow driven by RNO 15 FIR, with a p.a. of  $\sim 32^\circ$ . A jet from RNO 15 FIR, with an opening angle of only  $\sim 5^\circ$ , would encompass all of the emission from knots B and C. Knot A could also be driven by such a highly collimated jet, since it appears bow shock-shaped with the bow symmetry axis orientated along the flow axis.

We also mention the faint, though knotty, arc of H<sub>2</sub> line emission some 10'' to the west of knot B, and the faint H<sub>2</sub> emission in the southeast corner of the H<sub>2</sub> image (labelled in Fig. 9). These features appear to be unrelated to the RNO 15 FIR jet. Instead, they may be associated with a poorly collimated outflow from RNO 15: even though RNO 15 itself was not observed here, the red lobe of the CO outflow does encroach on the region imaged. Note, however, that the axis through the faint knots in the southeast corner of the image misses RNO 15 by about 20''.

#### 4. Discussion

In this section we use the data presented above to address some of the issues relevant to our understanding of outflows from young stars. We firstly consider the relationship between collimated stellar jets – which we see via molecular shocks formed between the jet and its surroundings, and their more poorly collimated molecular counterparts – which are usually mapped in CO. We then comment on whether flow variability plays a part in producing the H<sub>2</sub> shock structures observed in these outflows. Finally, we attempt to draw some general conclusions from the data as a whole.

##### 4.1. Jet-driven molecular outflows

There is growing support for the idea that molecular (CO) outflows are driven solely by collimated stellar jets, i.e. that there is no “unseen”, poorly collimated disk wind through which ambient molecular gas is being entrained (e.g. Masson & Chernin 1993; Chernin & Masson 1995). Two general models for jet driven outflows prevail. In the first, ambient, molecular gas is swept up through bow shocks that develop at the head of, or along the length of, a collimated jet. This swept up gas cools rapidly and, although some of the gas will spill down the sides of the jet, a dense “plug” of gas collects just behind each bow shock. This scenario is referred to as the bow shock or “prompt” entrainment model (Chernin et al. 1994; Masson & Chernin 1993; Raga & Cabrit 1993). In the second model, ambient gas is entrained along the length of the jet via a turbulent boundary layer (Taylor & Raga 1995; Raga, Cabrit & Cantó 1995; Stahler 1994). In this “steady-state” model, the turbulent layer will thicken with distance from the source, as more and more jet

gas and ambient gas is pulled into the layer. Eventually, the jet itself will be completely pinched off and the flow will become fully turbulent. With our H<sub>2</sub> observations of molecular outflows, can we now distinguish between these entrainment models, or at least identify which mechanism dominates?

Here we consider a simplification of the bow shock model. Davis, Eisloffel & Smith (1996) point out that, if a large fraction of the CO outflow represents ambient gas swept up in radiative bow shocks, then, assuming momentum balance, the radiative luminosity in these shocks is approximately equal to the mechanical power of the swept-up shocked gas. In other words, the energy radiated in the entraining shocks, which we assume is predominantly in H<sub>2</sub> ro-vibrational emission lines, should be comparable to the mechanical power in the molecular (CO) outflow. Unfortunately, only the HH 26 and L 1660 outflows have been mapped (in any detail) in CO (Gibb & Heaton 1993; Schwartz et al. 1988): we therefore compare the observed integrated H<sub>2</sub> luminosities to the mechanical power in the CO outflows in these two systems only (though for a similar analysis of a larger sample, see Davis & Eisloffel 1995).

From Gibb (1994), the power in the HH 26 CO outflow is estimated to be  $\sim 0.06 L_\odot$ . This compares to a total H<sub>2</sub> S(1) integrated flux (for knots HH 26A-D) of  $18.6 \times 10^{-16} \text{ W m}^{-2}$  which, at a distance of 400 pc, converts to  $0.009 L_\odot$ . If the H<sub>2</sub> S(1) line only represents about 1/10th of the total energy radiated in all the H<sub>2</sub> ro-vibrational lines, as seems reasonable (Smith 1995), then the total H<sub>2</sub> line luminosity is  $\sim 0.09 L_\odot$ . This value is remarkably close to the estimated mechanical power in the HH 26 CO outflow, considering the uncertainties inherent in calculating the CO outflow energetics (e.g. Snell et al. 1984). Also, we have not taken into account cooling from other molecules (like CO and H<sub>2</sub>O rotational and vibrational cooling), nor H<sub>2</sub> dissociative cooling. We have also not corrected the H<sub>2</sub> luminosity for extinction. In the map of Gibb & Heaton (1993), the compact HCO<sup>+</sup> core nearest to the HH 26 outflow, core F, has an estimated mean column density of  $\sim 3.6 \times 10^{23} \text{ cm}^{-2}$  (see also Gibb et al. 1995). This converts to 18 magnitudes of extinction at 2.12  $\mu\text{m}$  (following Davis & Eisloffel 1995). Where the HH 26 outflow crosses core F, we detect no H<sub>2</sub> emission: this suggests that the flow lies behind core F, so any H<sub>2</sub> shocks in this section of the outflow will be obscured. The total IR luminosity of the HH 26 outflow could therefore be a few times higher than the value given above. In any case, the H<sub>2</sub> data do suggest that the power radiated at near-IR wavelengths may be roughly equal to that transported in the CO outflow, as is predicted by this simple radiative shock model. The spatial coincidence between the observed H<sub>2</sub> shocks and the peaks in the CO outflow map of HH 26 (and indeed HH 25) also lend support to the bow shock entrainment model (Raga & Cabrit 1993; Chernin et al. 1994; Davis & Eisloffel 1995).

The integrated H<sub>2</sub> S(1) flux in knots HH 72A-L in L 1660 is  $4.1 \times 10^{-16} \text{ W m}^{-2}$ . At a distance of 1500 pc, the H<sub>2</sub> S(1) integrated flux converts to a luminosity of  $0.028 L_\odot$ , which is equivalent to a total H<sub>2</sub> luminosity (in all H<sub>2</sub> lines) of  $0.3 L_\odot$ . This luminosity is about three orders of magnitude lower than the estimated mechanical power in the high-velocity gas mapped

in CO by Schwartz et al. (1988). Taking into account other radiative cooling mechanisms (as described above) and, particularly, correcting the measured H<sub>2</sub> S(1) flux for extinction would increase our estimate of the radiative energy losses. Many of the H<sub>2</sub> knots are embedded within the L 1660 cloud core, so the H<sub>2</sub> features west of knot F will certainly be obscured (an  $A_v \sim 25$  would reduce the flux by a factor of 10). Also, as already mentioned, there are uncertainties associated with calculating the kinetic energy and, particularly, the dynamical age of the CO outflow (Snell et al. 1984). Indeed, recent statistical studies suggest that the dynamical ages of many molecular outflows, estimated from CO observations, are underestimates of the true outflow durations by as much as a factor of 10-100 (Parker, Padman & Scott 1991). A higher dynamical age, and subsequently a lower mechanical power in the high-velocity molecular outflow in L 1660, may well account for the discrepancy in H<sub>2</sub> luminosity to CO mechanical power reported here.

To conclude, then; in the HH 25, HH 26 and HH 72 molecular outflows, the association between the collimated jets traced in H<sub>2</sub> emission, and the molecular outflows observed in CO, implies that these outflows are indeed jet driven. Moreover, in HH 25 and HH 26, the spatial coincidence between the individual H<sub>2</sub> shocks (some of which appear to be bow shocks) and the peaks in the CO outflow lobes, together with the apparent equality between the mechanical power in the HH 26 outflow and the H<sub>2</sub> luminosity in the HH 26 shocks, all point to the radiative bow shock model as being the dominant entrainment mechanism.

#### 4.2. Variability in jets from young stars

Models of variable jets have been proposed to explain the sequences of knots observed in collimated, optical, Herbig-Haro jets (reviewed in Raga 1993). We now consider whether such models can realistically account for the molecular shocks observed, firstly in the L 1634 outflow, and then in the other outflows imaged here.

Pulsed jet models generate internal working surfaces along the jet beam, where faster sections of the jet catch up with, and shock, slower sections (Raga et al. 1990; Gouveia dal Pino & Benz 1994; Biro & Raga 1994;). Each working surface represents a layer of shocked jet gas that is bounded both upwind and downwind by a radiative shock. Spillage of the shocked gas from each layer in a direction perpendicular to the flow direction, and the subsequent “sweeping back” of this gas as it interacts with the ambient medium, will result in a bow shaped configuration for each leading, working surface shock (Biro 1996). These may appear much like the H<sub>2</sub> bow shocks in L 1634 (HH 240 A-D). However, pulsed jet models predict that bow shock sizes will increase with distance from the source (due to the continuous sideways expulsion of material, Gouveia dal Pino & Benz 1994); for HH 240A to HH 240D, the H<sub>2</sub> data suggest that the bows *decrease* in size with distance from the source.

Nevertheless, let us assume for the moment that the bow shocks in L 1634, labelled HH 240A-D in Fig. 5, are generated by a pulsed jet. If the velocity variation is a smooth function

of time, e.g. sinusoidal, then the distance to the first working surface is given by (Raga 1993)

$$x_v \sim \left( \frac{v^2}{2\Delta v} \right) \tau_v \quad (1)$$

where  $v$  is the average flow velocity along the jet,  $\Delta v$  the velocity amplitude variation and  $\tau_v$  the period. Assuming that HH 240A is the first working surface, and that the flow lies close to the plain of the sky (this seems likely since there is no overlap in the blue and red-shifted CO outflow lobes in Fig. 6), then a velocity  $v = 100 \text{ km s}^{-1}$  and a variation  $\Delta v = 10 \text{ km s}^{-1}$  predicts a period of about 500 years. At larger distances from the source, the working surfaces will move at a constant velocity (Kofman & Raga 1992) and be separated by a distance  $\Delta x = v\tau_v$ . The bow shocks HH 240B, 240C and 240D are more or less equally spaced along the flow axis, by about  $15''$  ( $10^{15} \text{ m}$ ). This spacing predicts a similar period for the velocity variation of roughly 320 years (again assuming  $v = 100 \text{ km s}^{-1}$ ).

Alternatively, it has recently been shown that even continuous jets can to some extent produce bow shocks along the flow axis (Suttner et al. 1996; Downes 1996). Radiative cooling at the bow head of a jet will result in the build-up of a clump or “plug” of dense molecular gas. This may eventually become detached, most probably through Raleigh-Taylor instabilities, and be swept upstream of the jet head. A bow shock may then form around this clump. The simulated H<sub>2</sub> maps of Suttner et al. (1996), generated from 3D molecular jet models, are rather similar to the image of L 1634 in Fig. 5. However, their models more closely match the data if the jet is variable (see their Fig. 15, which assumes a “wiggling” and pulsed jet). Suttner et al. also predict smaller bow shocks towards the end of the jet, as are observed in L 1634.

We find, therefore, that the well-defined bow shocks HH 240A-D in the L 1634 outflow are best explained with a variable-velocity jet model. The flow may also be slowly changing direction (wiggling), since the HH 240 and HH 241 knots do not all lie on the same axis. Spectroscopic data and proper motion studies would, however, enable us to better understand these remarkable molecular bow shocks.

What of the other outflows discussed in this paper? The rapid cooling ( $\sim$ few years) associated with these Herbig-Haro-like near-IR shocks, and the inhomogeneous, clumpy structure of the molecular environment surrounding each outflow, often leads to a rather complex picture in the near-IR. Shock features near the source may also be partially obscured from view by the protostellar cloud core. Of the other outflows observed, the simplest flow scenario appears to be that of RNO 15 FIR. Here, three colinear peaks of H<sub>2</sub> emission are observed along a well-defined flow axis, which also runs through the conical reflection nebula observed near the IRAS source position. However, these H<sub>2</sub> knots occur at random distances from the source, so there is no clear indication of periodic variations in velocity, or indeed direction, in this outflow.

In L 1660 the flow appears far more complex. Knots D, B and E (Fig. 8) could derive from a – now severely fragmented

– bow shock (perhaps fragmented because of thermal instabilities; e.g. Blondin, Königl & Fryxel 1989). Alternatively, and somewhat more speculatively, Knots B and E could represent two independent bow shocks, produced by the jet as it changes direction or “wiggles”. The other knots along the flow axis might then be caused by the underlying jet as it sways from side to side, splashing off the walls of the cavity swept out by the HH 72B and/or HH 72E working surfaces. If this is the case, then the positions of knots B and E suggest that the flow has turned through an angle of some  $7^\circ$  within a period given by  $t = (r_B - r_E)/V_{\text{bow}} = 3.2 \times 10^5 / V_{\text{bow}}$ , where  $t$  is in years and  $r_B$ ,  $r_E$  and  $V_{\text{bow}}$  are the radial distances and bow shock velocity (in  $\text{km s}^{-1}$ ) associated with knots B and E. Here we assume that, in time  $t$ , bow B has moved to its present location from a position directly south of bow E’s present location. A velocity of  $300 \text{ km s}^{-1}$  implies a period of  $\sim 10^4$  yrs.

In HH 25 we observe bright knots only near the ends of the flow lobes; these are probably associated with shock working surfaces, through which ambient gas is entrained to produce the observed CO outflow (Fig. 4). In HH 26 we see far more of the outflow in the near-IR. The knots along this curving flow axis appear clumpy (Fig. 3), although unlike many optical jets (Ray 1996), they are poorly aligned. This miss-alignment could again be due to wiggling of the jet, or indeed velocity variability. Higher resolution images, obtained with adaptive optics or *NICMOS* on the refurbished *HST* might lead to a better understanding of this and indeed the other outflows discussed in this paper.

#### 4.3. Near-IR outflow characteristics

Most of the outflows observed here are driven by deeply embedded and therefore potentially very young Class I or Class 0 sources (note that the HH 24-MMS, HH 25-MMS, L 1634, L 1660 and RNO 15 FIR sources are not detected at near-IR wavelengths). Do these flows have anything in common? In Table 5 we compare some of the characteristics of the outflows discussed in this paper with those of other flows that have been observed in the near-IR. Outflows are grouped depending on the evolutionary status of their exciting source, although some of the far-infrared sources (FIR) may yet be identified as being very young Class 0 sources. Outflows with sources observed at near-IR wavelengths are labelled ‘IR’, and, for comparison, we also list 3 outflows (at the bottom of the Table) that are associated with luminous star forming regions.

In Table 5 we give estimates for the total  $\text{H}_2$  luminosity in each outflow ( $\text{H}_2$  is probably the dominant coolant in molecular shocks in outflows; Neufeld & Kaufman 1993). We find a wide range of values for the  $\text{H}_2$  luminosity. Not surprisingly, the largest values are associated with the more energetic outflows from luminous sources. However, there is evidently no clear link between  $\text{H}_2$  luminosity and the *embeddedness* (as measured by IR excess; Bachiller 1996) of the exciting source. In other words, the outflows driven by sources that are probably more evolved (i.e. the IR sources in Table 5), where the flow may have blown away much of the ambient gas in the protostellar core, appear

to be neither more nor less luminous in  $\text{H}_2$  than their younger counterparts (the Class 0 sources).

The youngest source observed by us, HH 24-MMS, also appears to be associated with the *shortest* outflow (as traced in  $\text{H}_2$  line-emission). However, the  $\text{H}_2$  flows associated with the other potential Class 0 sources, such as HH 25-MMS (which lies in the same molecular cloud) and VLA 1623 (Dent et al. 1995), are comparable in projected length to the outflows from the more evolved sources. The apparent flow length (and consequently the integrated luminosity), derived from  $\text{H}_2$  observations, is therefore probably dictated by the extent and clumpiness of the cloud core that harbours each source, rather than the age of the source itself. This is perhaps not surprising, since once the outflow leaves the molecular cloud core there will be no ambient molecular material to shock-excite or entrain.

We finally comment on the fact that the sequence of sweeping bow shocks in L 1634 are qualitatively similar to those observed at optical wavelengths in for example HH 34, HH 111 (Reipurth 1989) and HH 24C-E (Mundt et al. 1991), while the fragmented bows in L 1660 (HH 72) are similar in appearance to, e.g., the optical bow shock HH 1 (Ray 1996). However, with the possible exception of the HH 24-MMS outflow, in the near-IR, we do not observe the underlying jet directly (i.e. as a sequence of closely-spaced knots), as we often do in optical images of Herbig-Haro flows (e.g. Mundt, Brugel & Bührke 1987). Instead, in  $\text{H}_2$  we observe molecular shocks driven into the surroundings by each jet, or the wings of sweeping bow shocks that accelerate and entrain ambient, molecular gas into the flow. Only in HH 24-MMS do we see evidence of an extended, collimated, knotty jet like that seen in, say, HH 1 or HH 34 (Ray 1996). Consequently, although the outflows themselves are enshrouded in dense, molecular gas, the underlying jet that drives the molecular outflow and powers the molecular shocks may be predominantly atomic and/or ionic, and either too diffuse or too warm to allow molecular reformation in abundance. Moreover, any optical emission generated in internal shocks formed along the jet axis will probably be obscured from view by the surrounding, natal cloud envelope.

## 5. Conclusions

We present near-infrared images of four YSO outflow regions, HH 24-26, L 1634, L 1660 and RN 15 FIR. The data reveal the many molecular shocks that form as the outflows interact with their surroundings. Indeed, it is likely that, in  $\text{H}_2$ , we are observing the molecular shocks which entrain ambient gas to form the associated CO outflows; these observations therefore provide evidence that CO outflows are driven by collimated stellar jets.

In the well-known HH 24-26 region, molecular outflows are observed towards the potentially very young sources, HH 24-MMS and HH 25-MMS. In  $\text{H}_2$ , all of the outflows are highly collimated, although surprisingly, the orientation of each flow appears to be completely random; there is certainly no evidence for outflows from the same cloud core being aligned.

The L 1634 and L 1660 outflows are probably more evolved than their counterparts in the HH 24-26 region. The L 1634 out-

**Table 5.** Characteristics of H<sub>2</sub> outflows

	Source Type	Source $L_{\text{bol}}$ ( $L_{\odot}$ )	Distance (pc)	Projected Length (pc)	$L_{\text{H}_2}^{\text{a}}$ ( $L_{\odot}$ )	Ref.
HH 24-MMS <sup>c</sup>	Class 0	5-20	400	0.02	0.002	1
VLA 1623	Class 0	1	160	0.7	0.016	2
L 1448-mm	Class 0	9	300	0.13	0.028	3,4
NGC 2264G	Class 0	12	800	0.41	0.12	5
Cep E	Class 0	100	1730	0.34 <sup>b</sup>	0.69 <sup>b</sup>	6
HH 25-MMS	Class 0/I	<10	400	0.33	0.051	1
HH 211	Class 0/I	–	300	0.15 <sup>b</sup>	0.03 <sup>b</sup>	7
HH 212	Class 0/I	–	470	0.5	0.07	8
L 1634	FIR	17	470	0.85	0.088	1
L 1660	FIR	170	1500	0.94	0.29	1
RNO 15 FIR	FIR	–	350	0.23	0.005	1
L 483	FIR	9	200	0.07	0.0006	9
L 1157	FIR	11	440	0.31 <sup>b</sup>	0.14 <sup>b</sup>	5
HH 111	FIR	24	470	0.34	0.007	10
HH 1/2	FIR	50	470	0.40 <sup>b</sup>	0.06 <sup>b</sup>	11
IRAS 03282	FIR	2	300	0.31	0.07	12,13
HH 7-11	IR	80	220	0.08	0.02	14
HH 26	IR	–	400	0.42	0.092	1
HH 43	IR	3.6	470	0.14	0.035	15
HH 46/47	IR	19	460	0.57 <sup>b</sup>	0.011 <sup>b</sup>	16
NGC 6334I	IR	–	1740	0.37	0.69	5
Haro 4-255	IR	13	480	0.24	0.0012	5
HH 33/40 <sup>d</sup>	–	–	470	0.16	0.02	17
HH 91	–	–	470	1.3 <sup>b</sup>	0.18 <sup>b</sup>	10
HH 110	–	–	470	0.45	0.008	10
Cep A	–	$2.5 \times 10^4$	725	0.5	0.6	18
DR 21	–	$2.5 \times 10^5$	3000	5.0 <sup>b</sup>	1.8 <sup>b</sup>	19
IRAS 21334	IR	$2.5 \times 10^4$	5000	2.1 <sup>b</sup>	8.0 <sup>b</sup>	20

<sup>a</sup>Luminosity in all H<sub>2</sub> ro-vibrational lines, assuming  $L_{\text{H}_2} = 10 \times F_{\text{S}(1)} \times 4\pi d^2$ , where  $F_{\text{S}(1)}$  is the integrated H<sub>2</sub> S(1) flux and  $d$  is the distance to the source.

<sup>b</sup>Includes both outflow lobes.

<sup>c</sup>Excluding HH 24A.

<sup>d</sup>Bally & Devine (1994) suggest that HH 33-40 may be only a small part of a much larger outflow centred on HH 34.

References: 1. This paper; 2. Dent, Matthews & Walther 1995; 3. Bally, Lada & Lane 1993a; 4. Davis et al. 1994a; 5. Davis & Eislöffel 1995; 6. Eislöffel et al. 1996; 7. McCaughrean, Rayner & Zinnecker 1994; 8. Zinnecker, McCaughrean & Rayner 1996; 9. Fuller et al. 1995; 10. Davis, Mundt & Eislöffel 1994b; 11. Davis, Eislöffel & Ray 1994c; 12. Bally et al. 1993b; 13. Bachiller et al. 1994; 14. Stapelfeldt et al. 1991; 15. Gredel 1995; 16. Eislöffel et al. 1994; 17. Zealey et al. 1992; 18. Hartigan et al. 1996; 19. Davis & Smith 1996; 20. Smith & Fisher 1992.

flow exhibits some degree of symmetry in that the spectacular bow shocks in the western, blue-shifted lobe are matched by similar, though less well defined structures in the counter-flow. These structures hint at variability in the flow velocity and direction. In L 1660, however, the outflow appears less well ordered and more poorly collimated. We also report the discovery of a sequence of compact H<sub>2</sub> knots in the RNO 15 FIR region. These shock features delineate a highly collimated jet from this FIR source.

Finally, based on the sample of outflows observed here, and H<sub>2</sub> observations of other outflows found in the literature, we

conclude that the luminosity (in H<sub>2</sub>) and extent of each H<sub>2</sub> flow is not dependent on the embeddedness of the source, but rather that they depend on the extent and clumpiness of the cloud core that harbours each source.

*Acknowledgements.* We would like to thank Andy Gibb for supplying us with, and allowing us to reproduce, his CO maps of the HH 25-26 outflows, and A. Mizuno for kindly sharing his L 1634 CO data with us prior to publication. We also thank Mike Smith and Turlough Downes for their comments on jets and H<sub>2</sub> excitation, the staff at UKIRT for their support during the observations, and the JCMT service observing team for promptly supplying us with the submillimetre data. The United

Kingdom Infrared Telescope (UKIRT) is operated by the Royal Observatories on behalf of the UK Particle Physics and Astronomy Research Council (PPARC). The James Clerk Maxwell Telescope is operated by The Observatories on behalf of PPARC, the Netherlands Organisation for Scientific Research, and the National Research Council of Canada. Finally, this research has made use of the Digitised Sky Survey plates available via *Skyview* on the internet and the Simbad database, operated at CDS, Strasbourg, France.

## References

- André, P., Ward-Thompson, D., Barsony, M. 1993, *ApJ* 406, 122
- Anthony-Twarog, B.J. 1982, *AJ*, 87, 1213
- Bachiller, R., 1996, *A&A*, 34, 111
- Bachiller, R., Cernicharo, J., Martín-Pintado, J., Tafalla, M., Lazareff, B., 1990, *A&A* 231, 174
- Bachiller, R., Terebey, S., Jarrett, T. et al., 1994, *ApJ*, 437, 296
- Bally, J., Devine, D., 1994, *ApJ* 428, L65
- Bally, J., Devine, D., Hereld, M., Rauscher, B.J. 1993b, *ApJ*, 418, L75
- Bally, J., Lada, E.A., Lane, A.P. 1993a, *ApJ*, 418, 322
- Biro, S., 1996, *MNRAS* 278, 990
- Biro, S., Raga, A., 1994, *ApJ* 434, 221
- Blondin, J.M., Königl, A., Fryxell, B.A., 1989, *ApJ* 337, L37
- Bohigas, J., Persi, P., Tapia, M., 1993, *A&A* 267, 168
- Bontemps, S., André, P., Ward-Thompson, D., 1995, *A&A* 297, 98
- Bontemps, S., Ward-Thompson, D., André, P., 1996, *A&A* 314, 477
- Chandler, C.J., Koerner, D.W., Sargent A.I., Wood D.O.S., 1995, *ApJ* 449, L139
- Chernin, L., Masson, C., 1995, *ApJ* 455, 182
- Chernin, L., Masson, C., Gouveia Dal Pino, E.M., Benz, W., 1994, *ApJ* 426, 204
- Chini, R., Krügel, E., Haslam, C.G.T. et al., 1993, *A&A* 272, L5
- Cohen, M., Harvey, P.M., Schwartz, R.D., 1985, *ApJ* 296, 633
- Davis, C.J., Dent, W.R.F., Matthews, H.E., Aspin, C., Lightfoot, J.F., 1994a, *MNRAS* 266, 933
- Davis, C.J., Eisloffel, J., 1995, *A&A* 300, 851 (Erratum; *A&A* 305, 694)
- Davis, C.J., Eisloffel, J., Smith M.D., 1996, *ApJ* 463, 246
- Davis, C.J., Eisloffel, J., Ray, T.P., 1994c, *ApJ* 426, L93
- Davis, C.J., Mundt, R., Eisloffel, J. 1994b, *ApJ*, 437, L55
- Davis, C.J., Smith, M.D., 1995, *ApJ* 443, L41
- Davis, C.J., Smith, M.D., 1996, *A&A* 310, 961
- Dent, W.R.F., Matthews, H.E.M., Walther, D., 1995, *MNRAS* 277, 193
- Downes, T.P., 1996, *Astrophys. Letters and Communications*, 34, 309
- Eisloffel, J., Davis, C.J., Ray, T.P., Mundt, R., 1994 *ApJ*, 422, L91
- Eisloffel, J., Smith, M.D., Davis, C.J., Ray, T.P., 1996, *AJ*, 112, 2086
- Fukui, Y., 1989, in *Low Mass Star Formation and Pre Main Sequence Objects*, ed. B. Reipurth (ESO: Garching), p.95
- Fuller, G.A., Lada, E.A., Masson, C.M., Myers, P.C., 1995, *ApJ* 453, 754
- Gibb, A.G., 1994, Ph.D. Thesis (University of Kent at Canterbury), p.109
- Gibb, A.G., Davis, C.J., 1997, in preparation
- Gibb, A.G., Heaton, B.D., 1993, *A&A*, 276, 511
- Gibb, A.G., Little, L.T., Heaton, B.D., Lehtinen, K.K., 1995, *MNRAS* 277, 341
- Goldsmith, P.F., Snell, R.L., Hemeon-Heyer, M., Langer, W.D., 1984, *ApJ* 286, 599
- Gouveia Dal Pino, E.M., Benz, W., 1994, *ApJ* 435, 261
- Gredel, R., 1995, *A&A* 292, 580
- Hartigan, P., Carpenter, J.M., Dougados, C., Skrutskie, M.F., 1996, *AJ* 111, 1278
- Herbig, G.H., Jones, B.F., 1983, *AJ* 88, 1040
- Hilton, J., Lahulla, J.F., 1995, *A&AS* 113, 325
- Hodapp, K.-W., 1994, *ApJS* 94, 615
- Hodapp, K.-W., Ladd, E.F., 1995, *ApJ* 453, 715
- Jones, B.F., Cohen, M., Sirk, M., Jarrett, R., 1984, *AJ* 89, 1404
- Jones, B.F., Cohen, M., Wehinger, P.A., Gehren, T., 1987, *AJ* 94, 1260
- Kofman, L., Raga, A.C., 1992, *ApJ* 390, 359
- Levreault, R.M., 1988, *ApJS* 67, 283
- Masson, C.R., Chermín, L.M., 1993, *ApJ* 414, 230
- McCaughrean, M.J., Rayner, J.T., Zinnecker, H., 1994, *ApJ* 436, L189
- Mundt, R., Brugel, E.W., Bührke, T., 1987, *ApJ* 319, 275
- Mundt, R., Ray, T.P., Raga, A.C., 1991, *A&A* 252, 740
- Neufeld, D.A., Kaufman, M.J., 1993, *ApJ* 418, 263
- Parker, N.D., Padman, R., Scott, P.F., 1991, *MNRAS* 252, 442
- Raga, A.C., 1993, *Ap&SS* 208, 163
- Raga, A.C., Cabrit, S., 1993, *A&A* 278, 267
- Raga, A.C., Cabrit, S., Cantó, J., 1995, *MNRAS* 273, 422
- Raga, A.C., Cantó, J., Binette, L., Calvet, N., 1990, *ApJ* 364, 601
- Ray, T.P., 1996, in *Solar and Astrophysical Magnetohydrodynamical Flows*, ed. K.C. Tsinganos, (Kluwer:Dordrecht), p.539
- Reipurth, B., 1989, In *Low Mass Star Formation and Pre-main sequence objects*, eds. B. Reipurth, (ESO: Garching), p.247
- Reipurth, B., 1994, in *A General Catalogue of Herbig-Haro Objects*, published electronically via anon. ftp to ftp.hq.eso.org, directory /pub/Catalogs/Herbig-Haro
- Reipurth, B., Chini, R., Krügel, E., Kreysa, E., Sievers, A., 1993, *A&A* 273, 221
- Reipurth, B., Graham, J.A., 1988, *A&A* 202, 219
- Schwartz, R.D., Cohen, M., Williams, P.M., 1987, *ApJ* 322, 403
- Schwartz, R.D., Gee, G., Huang, Y.-L., 1988, *ApJ* 327, 350
- Smith, M.D., 1995, *A&A* 296, 789
- Smith, H.A., Fisher, J., 1992, *ApJ* 398, L99
- Snell, R.L., Scoville, N.Z., Sanders, D.B., Erickson, N.R., 1984, *ApJ* 284, 176
- Solf, J., 1987, *A&A* 184, 322
- Stahler, S.W., 1994, *ApJ* 422, 616
- Stapelfeldt, K.R., Beichman, C.A., Hester, J.J., Scoville, N.Z., Gautier, T.N. 1991, *ApJ*, 371, 226
- Strom, K.M., Strom, S.E., Vrba, F.J., 1976, *AJ* 81, 308
- Suttner, G., Smith, M.D., Yorke, H.W., Zinnecker, H., 1996, *A&A*, in press
- Taylor, S.D., Raga, A.C., 1995, *A&A* 296, 823
- Verdes-Montenegro, L., Ho, P.T.P., 1996, *ApJ* 473, 926
- Ward-Thompson, D., Chini, R., Krügel, E., André, P., Bontemps, S., 1995, *MNRAS* 274, 1219
- Zealey, W.J., Williams, P.M., Sandell, G., Taylor, K.N.R., Ray, T.P., 1992, *A&A* 262, 570
- Zinnecker, H., McCaughrean, M.J., Rayner, J.T., 1996, in *Disks & Outflows Around Young Stars*, eds. S.V.B. Beckwith, in press